Supporting information

PVD Customized 2D Porous Amorphous Silicon Nanoflakes Percolated with Carbon Nanotubes for High Areal Capacity Lithium Ion Batteries

Zhouhao Wang[a], Yan Li[a], Shaozhuan Huang[a,*], Lixiang Liu[b], Ye Wang[c], Jun Jin[d], Dezhi Kong[c], Lin Zhang[b], Oliver G. Schmidt[b,e]

[a]*Key Laboratory of Catalysis and Energy Materials Chemistry of Ministry of Education, South-Central University for Nationalities, Wuhan, Hubei, 430074, China, E-mail: husz001@scuec.edu.cn*

[b]*Institute for Integrative Nanosciences, Leibniz Institute for Solid State and Materials Research Dresden, Helmholtzstraße 20, Dresden, 01069 Germany*

[c]*School of Physics and Microelectronics, Zhengzhou University, Zhengzhou, Henan, China*

[d]*Faculty of Materials Science and Chemistry, China University of Geosciences, Wuhan, 430074, China*

[e]*Material Systems for Nanoelectronics, Technische Universität Chemnitz, Germany*

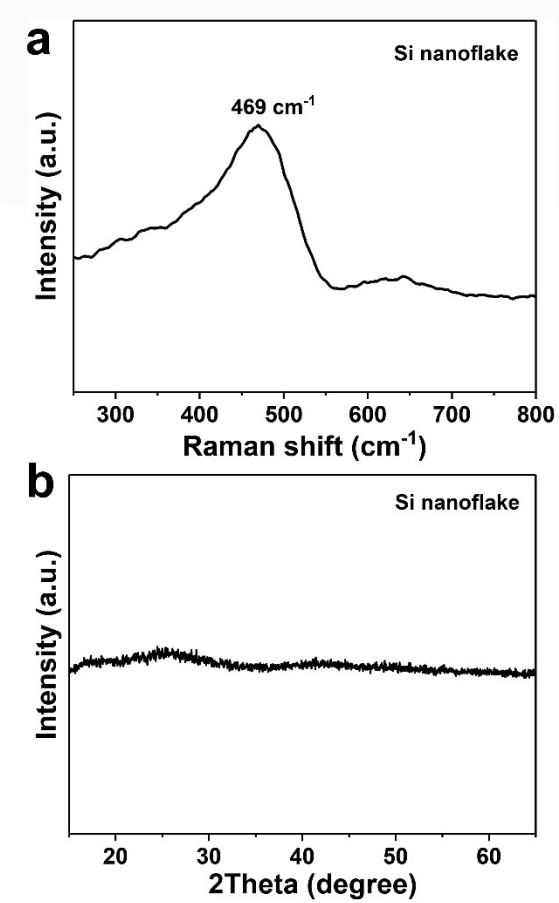

Figure S1. (a) Raman spectrum of Si nanoflakes, (b) XRD pattern of Si nanoflakes.

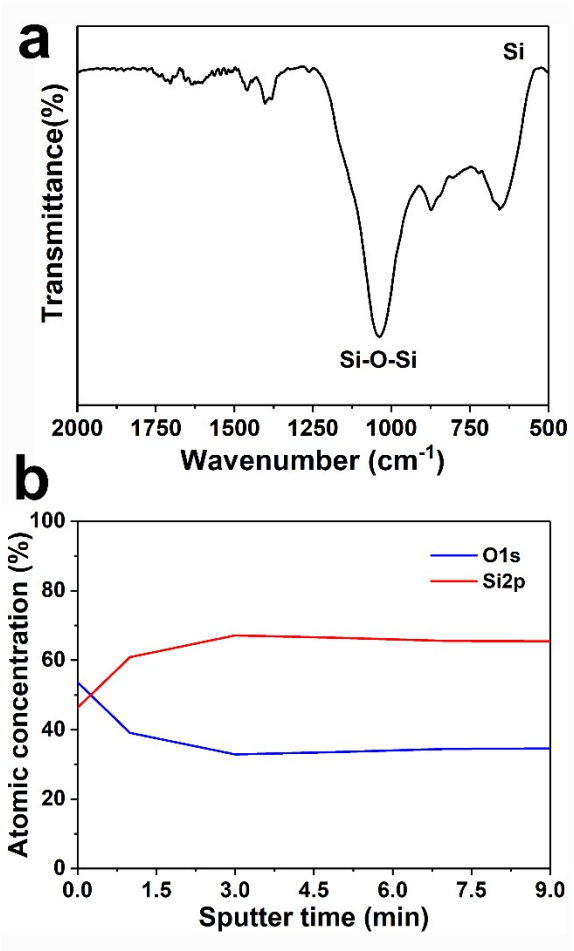

Figure S2. (a) FT-IR spectrum of amorphous Si nanoflake, (b) XPS depth profiling of Si 2p and O 1s performed on amorphous Si nanoflake.

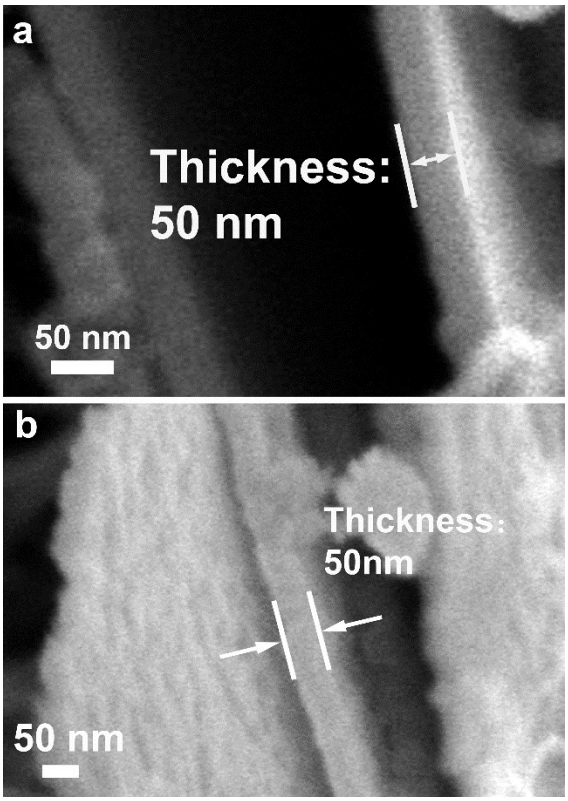

Figure S3. Cross sectional SEM image of pristine Si nanoflake (a), and porous Si nanoflake after $NH_3 \cdot H_2O$ treatment.

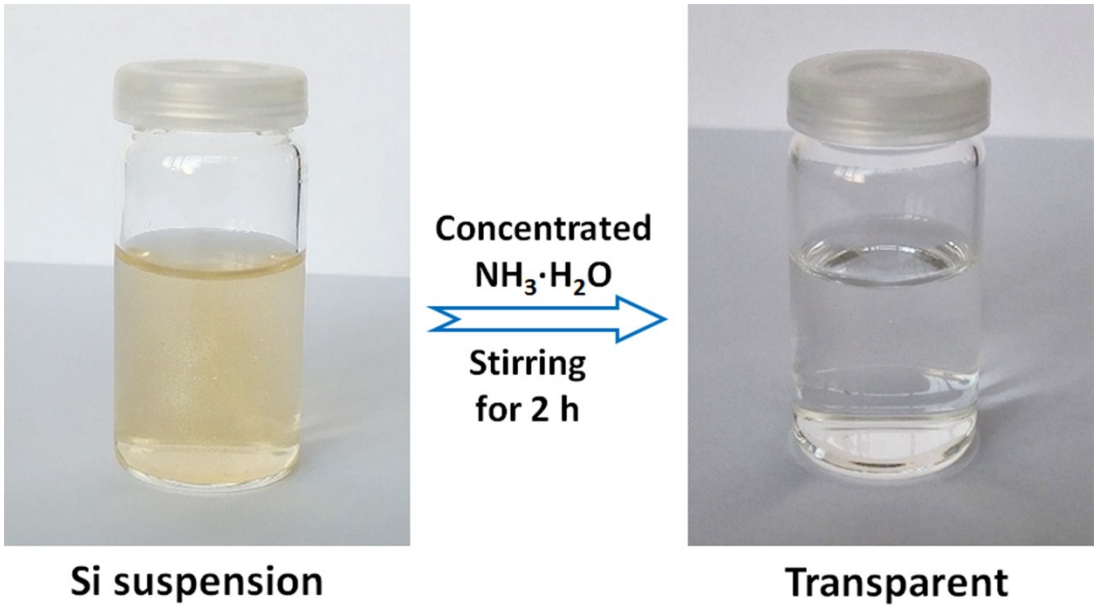

Figure S4. Digital picture of the Si suspension before/after reaction.

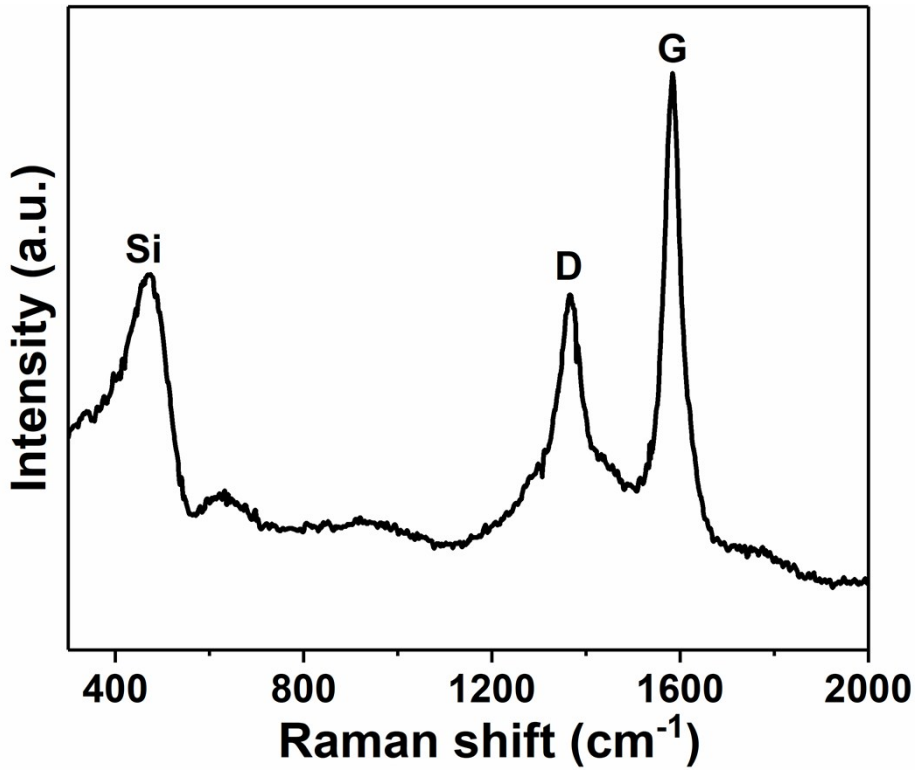

Figure S5. Raman spectrum of Si-MWCNTs membrane.

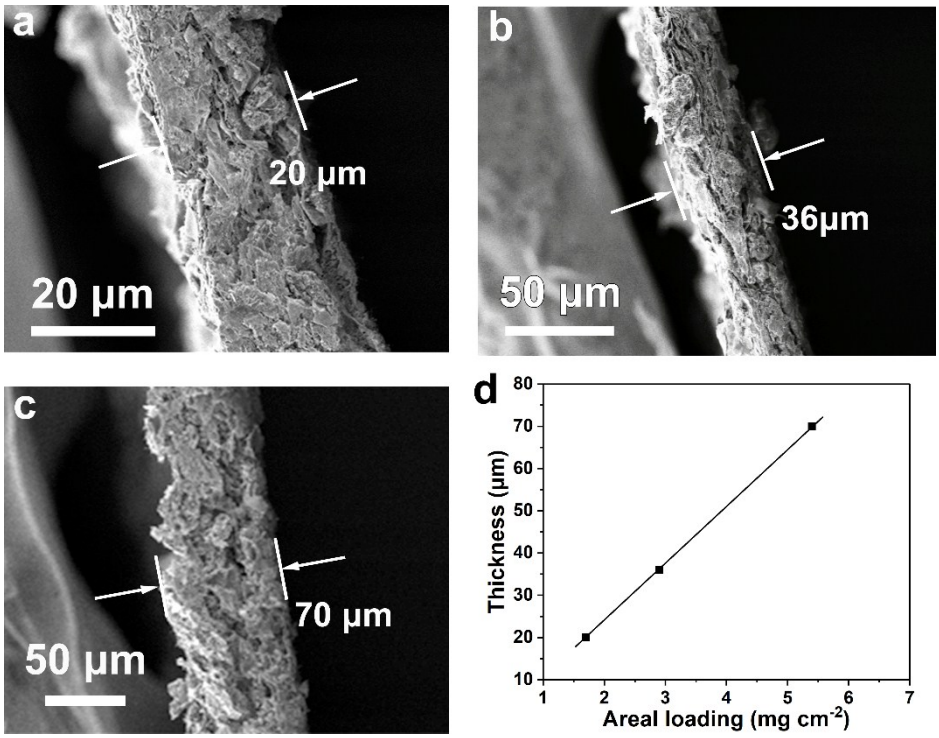

Figure S6. (a-c) Cross sectional SEM images of the Si-MWCNTs membranes with different thicknesses. (d) Relationship between the thickness and areal loading.

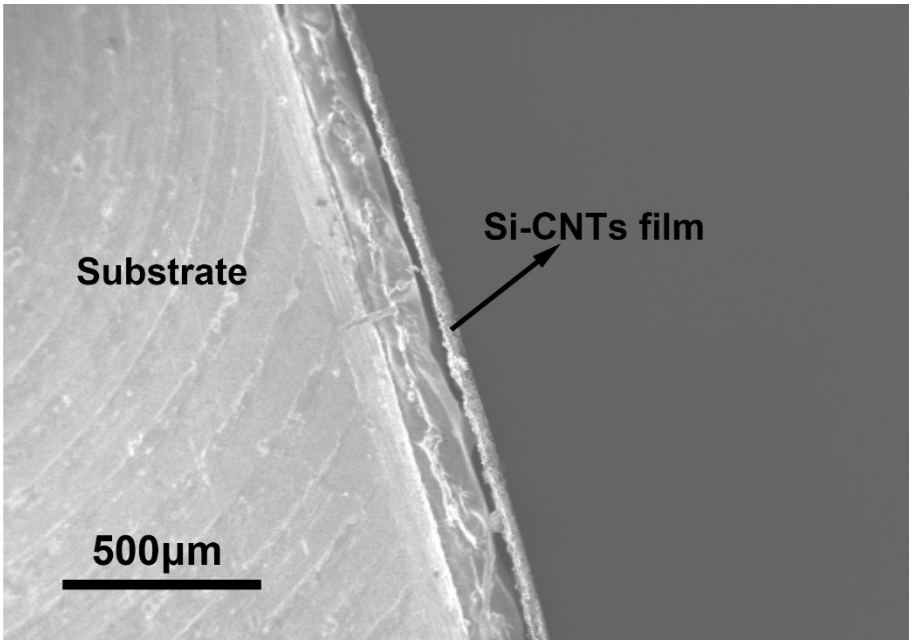

Figure S7. Low magnification cross sectional SEM image of Si-MWCTN film.

Table S1. Comparison of the mass loading and areal capacity based on Si-based film electrodes.

Samples	**Areal loading (mg cm^{-2})**	**Areal capacity (mAh cm^{-2})**	**Ref**
Si-MWCNTs	2.9	4.5	This work
Carbon-Coated Si	0.5	1.4	[1]
Carbon Graphdiyne Coated Si	1.28	4.72	[2]
Si/carbon nanofibers	0.76	0.66	[3]
Si/MXene Paper	1.3	3.8	[4]
Si/Carbon Fibers	2.0	2.4	[5]
Si/Carbon Fibers	4.65	4.0	[6]
Si/graphene membrane	0.4	0.69	[7]

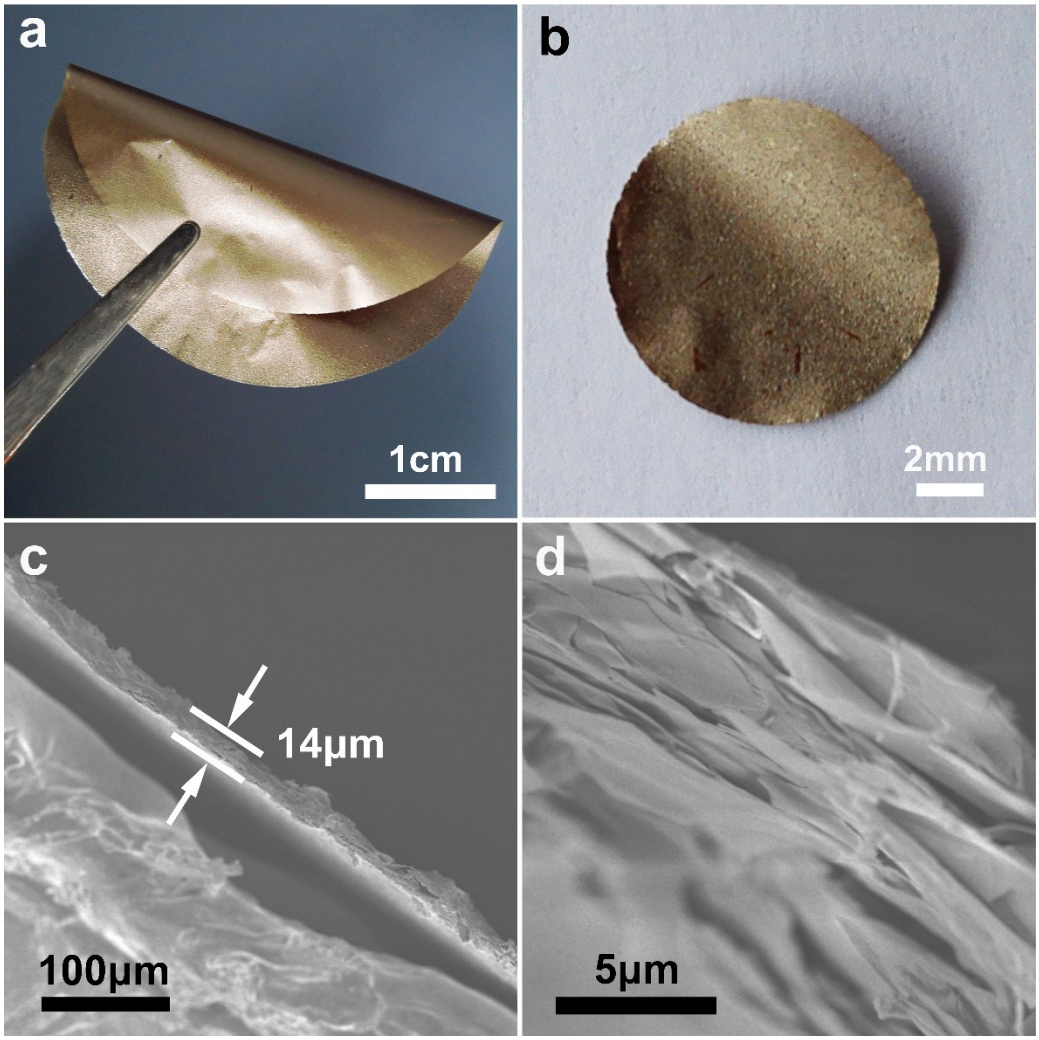

Figure S8. (a-b) Digital photo illustration of the freestanding Si film, (c-d) cross sectional SEM images.

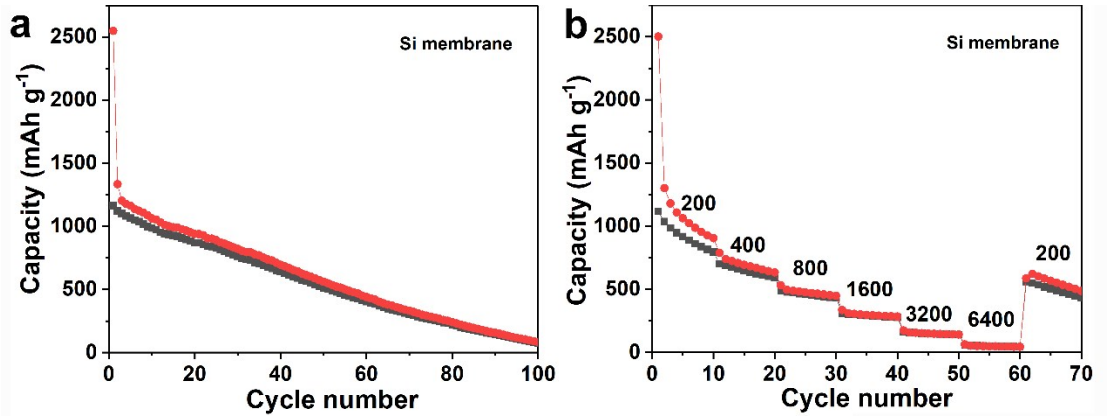

Figure S9. Electrochemical performance of Si membrane: (a) cycling performance at 200 mA g^{-1}, (b) rate capability.

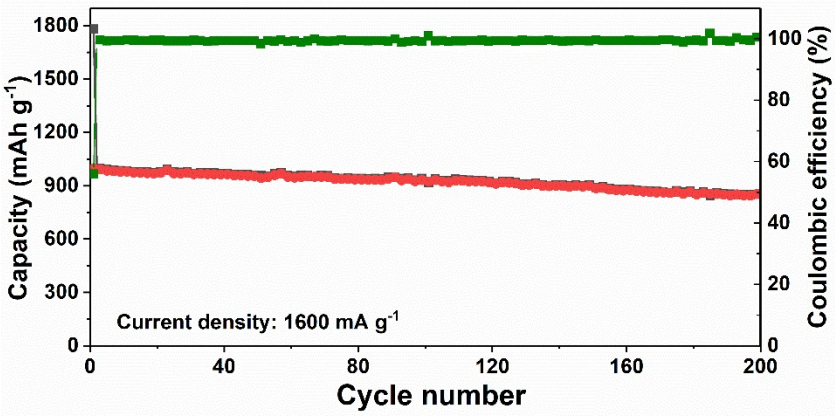

Figure S10. Long-term cycling of Si-MWCNTs film at 1600 mA g^{-1}, showing a capacity retention of 84.7% after 200 cycles.

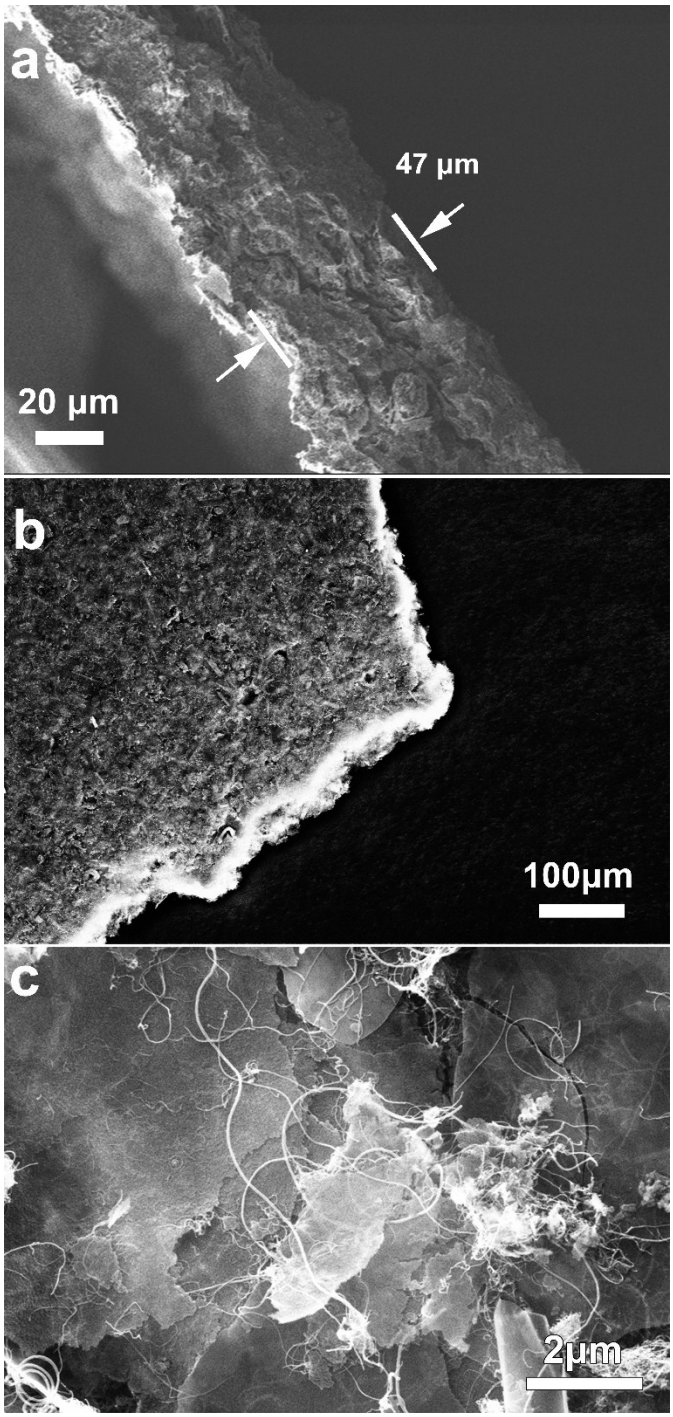

Figure S11. (a) Cross sectional SEM image of Si-MWCNT film after first lithiation. (b-c) *Ex-situ* SEM images of Si-MWCNT film after 100 cycles.

Table S2. Comparison of the smaple/electrode preparation and electrode mass loading of the Si nanosheets based electrodes.

Samples	Sample preparation	Phase structure	Electrode Preparation	Areal loading (mg cm^{-2})	Areal capacity (mAh cm^{-2})	Ref
Porous Si nanoflakes	PVD	Amorphous	Freestanding	2.9	4.5	This work
Si nanosheets	CVD	Crystalline	Slurry coating	1.5	1.9	[8]
2D silicon	physical vacuum distillation	Crystalline	Slurry coating	2	3.0	[9]
Few-Layer Silicene Nanosheets	liquid oxidation and exfoliation	Crystalline	Slurry coating	1.1	0.8	[10]
Silicon Nanosheets	CVD	Crystalline	Slurry coating	--	--	[11]
Silicon Nanosheets	Topochemical reaction	Amorphous	Slurry coating	2	2.0	[12]
2D silicon	CVD	Crystalline	Slurry coating	1.1	2.2	[13]

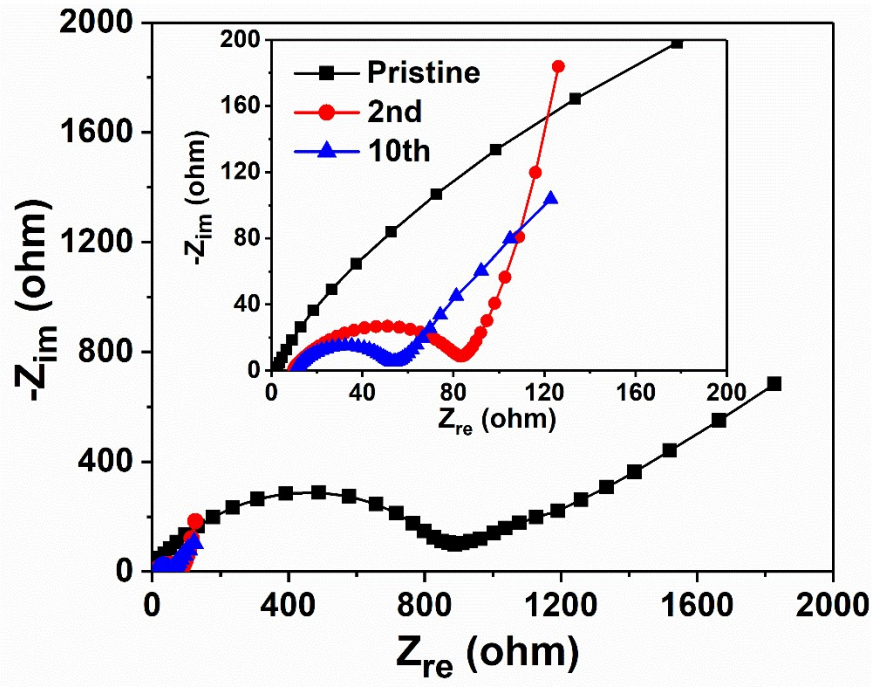

Figure S12. Nyquist plots of Si-MWCNTs at 200 mA g^{-1} at different cycles.

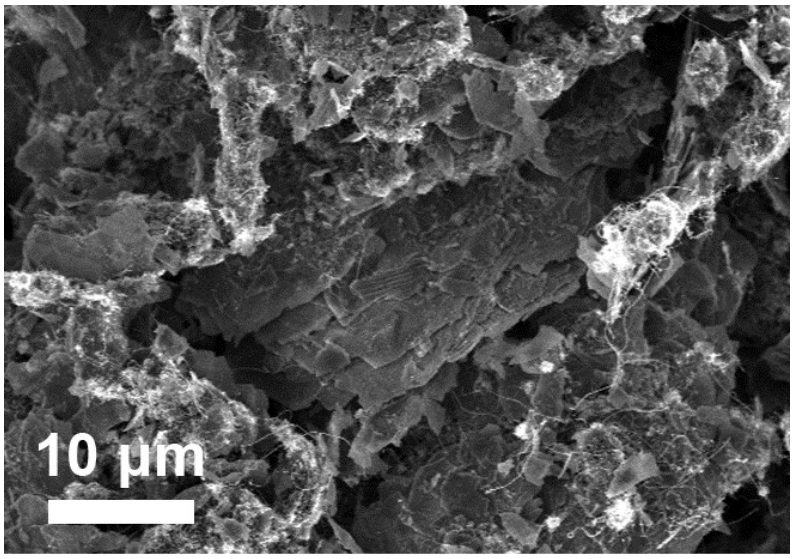

Figure S13. Ex situ SEM image of Si-MWCNTs at a high loading of 5.4 mg cm^{-2} after 100 cycles.

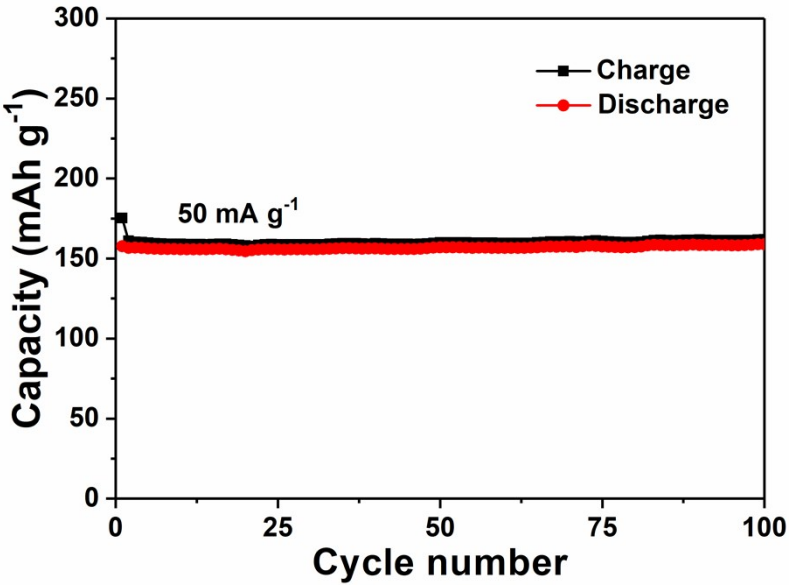

Figure S14. Cycling performance of NCM at 50 mA g^{-1}, showing a highly stable cycling.

References:

1 C. Shen, X. Fang, M. Ge, A. Zhang, Y. Liu, Y. Ma, M. Mecklenburg, X. Nie and C. Zhou, *ACS Nano,* 2018, **12**, 6280-6291.

2 H. Shang, Z. Zuo, L. Yu, F. Wang, F. He and Y. Li, *Adv. Mater.,* 2018, **30**, 1801459.

3 E. Qu, T. Chen, Q. Xiao, G. Lei and Z. Li, *J. Power Sources,* 2018, **403**, 103-108.

4 Y. Tian, Y. An and J. Feng, *ACS Appl. Mater. Interfaces,* 2019, **11**, 10004-10011.

5 X. Chen, P. Hu, J. Xiang, R. Zhang and Y. Huang, *ACS Appl. Energy Mater.,* 2019, **2**, 5214-5218.

6 M. Wang, W. Song, J. Wang and L. Fan, *Carbon,* 2015, **82**, 337-345.

7 Z. Luo, Q. Xiao, G. Lei, Z. Li and C. Tang, *Carbon,* 2016, **98**, 373-380.

8 J. Ryu, D. Hong, S. Choi and S. Park, *ACS Nano,* 2016, **10**, 2843-2851.

9 Y. An, Y. Tian, C. Wei, H. Jiang, B. Xi, S. Xiong, J. Feng and Y. Qian, *ACS Nano,* 2019, 13, 13690-13701.

10 J. Liu, Y. Yang, P. Lyu, P. Nachtigall and Y. Xu, *Adv. Mater.,* 2018, **30**, 1800838.

11 Z. Lu, J. Zhu, D. Sim, W. Zhou, W. Shi, H. H. Hng and Q. Yan, *Chem. Mater.,* 2011, **23**, 5293-5295.

12 K. Xu, L. Ben, H. Li and X. Huang, *Nano Res.,* 2015, **8**, 2654–2662.

13 J. Ryu, T. Chen, T. Bok, G. Song, J. Ma, C. Hwang, L. Luo, H.-K. Song, J. Cho and C. Wang, *Nat. Commun.,* 2018, **9**, 2924.